Reprinted from LANGMUIR, 1994, 10.

Shear Melting of Colloidal Crystals of Charged Spheres Studied with Rheology and Polarizing Microscopy

A. Imhof,* A. van Blaaderen, and J. K. G. Dhont

Van't Hoff Laboratory, Utrecht University, Padualaan 8, 3584 CH Utrecht, The Netherlands

Received April 1, 1994. In Final Form: July 18, 1994[⊗]

The effect of a shear flow on a colloidal crystalline phase of charge stabilized silica spheres was examined both by rheological measurements and by observing the process with a polarizing microscope. The microscopical observations show that a flow breaks up the crystal phase into crystalline regions coexisting with "shear melted" regions. Increasing the flow rate causes the shear melted regions to grow at the expense of the crystalline regions. In rheological experiments this transition occurs when on increasing the shear rate a critical shear stress is reached. During the transition the stress does not increase with shear rate until the entire crystalline phase has melted. The critical stress divided by the high-frequency limit of the storage modulus assumes a constant value independent of volume fraction and ionic strength.

1. Introduction

Colloidal dispersions of uniformly sized spherical particles display an interesting phase behavior. At a low volume fraction ϕ, the particles show a disordered liquidlike structure. When the volume fraction is increased to the so-called freezing volume fraction ϕ_f, an ordered crystalline phase can coexist with the liquid phase. Above the melting volume fraction ϕ_m the complete system assumes crystalline order. The equilibrium crystal structure is usually face centered cubic (fcc) but if the volume fraction is low enough a body centered cubic structure (bcc) dominates.[1,2] Finally, above the volume fraction for glass formation ϕ_g the motion of particles becomes so much hindered that the formation of the crystalline phase takes an "infinite" time and a disordered glassy structure remains.[3] For charge stabilized colloids we can, in addition to the volume fraction, also vary the ionic strength of the solvent. Decreasing the ionic strength effectively increases the range over which the particles interact, causing the phase transitions to occur at a lower volume fraction. The dispersion structure determines, among other things, the rheological properties of the dispersion and is itself, in turn, affected by the flow as a function of shear rate. The relation between structure and rheology is complicated; much work has been done and remains to be done.

In this paper we will be mainly concerned with the effect of a shear flow on a phase that is completely crystalline in equilibrium, that is $\phi > \phi_m$. The evolution of structure with increasing shear rate is then usually referred to as shear induced melting, since the structure is generally degraded in several steps from a long-range three-dimensional order to a disordered structure. Studies undertaken to establish the sequence of structures as a function of shear rate have mainly made use of scattering techniques.[4-11] These studies generally agree that the crystalline order is transformed into a two-dimensional structure consisting of freely sliding, hexagonally packed layers. In addition, Ackerson *et al.*[7,8] report, that at the lowest shear rates first a registered slipping of layers oriented to resist shear flow exists. At higher shear rates the sliding layers are usually seen to melt into a disordered liquidlike structure,[4,7,8] although Tomita and van de Ven[6] observed a layer ordering parallel to the flow for all shear rates. Yan and Dhont,[11] however, report for (probably) fcc crystals that the amorphous structure is preceded by an ordering into strings, which is also seen for low volume fraction bcc crystals.[5] Finally, Hoffman[4] reported a return of the sliding layers structure at very high shear rates.

Structural transitions are expected to be reflected in the rheological behavior of the dispersion, giving rise to sudden changes in the shear viscosity. These effects may be rather small, especially at the lower volume fractions. Another difficulty is the need for a colloid that crystallizes sufficiently rapidly. A considerable number of studies are aimed at the rheological properties of colloidal crystals in equilibrium (that is elastic moduli or dynamic rigidity; see *e.g.* refs 12-14. Fewer results are available on the rheology of shear or strain melting.[15-17] Still fewer studies combine rheology with structure determination,[4,10] allowing a direct comparison between structure and flow properties.

The present work is a contribution to the bridging of this gap. We show how a discontinuity in the flow of a colloidal crystal of charged silica spheres, seen recently for the first time by Chen and Zukoski[17] for an aqueous latex, is related to a transition in the dispersion structure. We report rheological measurements both of the steady shear during the transition and for the viscoelastic properties. Instead of scattering, however, we use a polarizing microscope to observe shear melting of the crystal in the shear/velocity plane. This technique has been shown to be very well suited for the observation of

[⊗] Abstract published in *Advance ACS Abstracts,* September 1, 1994.

(1) Williams, R.; Crandall, R. S. *Phys. Lett. A* **1974**, *48*, 225.
(2) Monovoukas, Y.; Gast, A. P. *J. Colloid Interface Sci.* **1989**, *128*, 533.
(3) van Megen, W.; Underwood, S. M. *Nature* **1993**, *362*, 616.
(4) Hoffman, R. L. *Trans. Soc. Rheol.* **1972**, *16*, 155; *J. Colloid Interface Sci.* **1974**, *46*, 491.
(5) Ackerson, B. J.; Clark, N. A. *Phys. Rev. Lett.* **1981**, *46*, 123; *Phys. Rev. A* **1984**, *30*, 906.
(6) Tomita, M.; van de Ven, T. G. M. *J. Colloid Interface Sci.* **1984**, *99*, 374.
(7) Ackerson, B. J.; Hayter, J. B.; Clark, N. A.; Cotter, L. *J. Chem. Phys.* **1986**, *84*, 2344.
(8) Ackerson, B. J. *J. Rheol.* **1990**, *34*, 553.
(9) Ashdown, S.; Markovic, I.; Ottewill, R. H.; Lindner, P.; Oberthür, R. C.; Rennie, A. R. *Langmuir* **1990**, *6*, 303.
(10) Chen, L. B.; Zukoski, C. F.; Ackerson, B. J.; Hanley, H. J. M.; Straty, G. C.; Barker, J.; Glinka, C. J. *Phys. Rev. Lett.* **1992**, *69*, 688.
(11) Yan, Y. D.; Dhont, J. K. G. *Physica A* **1993**, *198*, 78.
(12) Mitaku, S.; Ohtsuki, T.; Okano, K. *Jpn. J. Appl. Phys.* **1980**, *19*, 439.
(13) Benzing, D. W.; Russel, W. B. *J. Colloid Interface Sci.* **1981**, *83*, 178.
(14) Buscall, R.; Goodwin, J. W.; Hawkins, M. W.; Ottewill, R. H. *J. Chem. Soc., Faraday Trans. 1* **1982**, *78*, 2873, 2889.
(15) Lindsay, H. M.; Chaikin, P. M. *J. Phys. (Paris) C3* **1985**, *46*, 269.
(16) Bradbury, A.; Goodwin, J. W.; Hughes, R. W. *Langmuir* **1992**, *8*, 2863.
(17) Chen, L. B.; Zukoski, C. F. *J. Chem. Soc., Faraday Trans. 1* **1990**, *86*, 2629.

0743-7463/94/2410-3477$04.50/0

Table 1. Some Properties of the Solvents Used

[LiCl] (M)	conductivity (S/m)	κa
1.35×10^{-5}	1.08×10^{-4}	3.33
2.01×10^{-4}	1.43×10^{-3}	13.5
1.00×10^{-3}	6.29×10^{-3}	29.9

equilibrium colloidal crystals.[18] We show that it is also useful for the observation of the morphology of a crystalline phase depending on the shear history. Control of the morphology and flow properties of crystalline dispersions may become an important tool for the preparation of, for example, high-quality ceramics.

In section 2 we will describe the experimental procedures. The results will follow in section 3. In section 4 we will discuss the results and interpret the rheological data with the help of the microscopical observations. Finally, in section 5 our conclusions will be summarized.

2. Experimental Section

2.1. Preparation and Characterization of the Colloidal Silica System. We prepared the colloidal silica spheres, laboratory code FSA7(3), following the method of Stöber *et al.*[19] Although it was unnecessary for the work in this paper, the particles were fluorescently labeled using the synthesis described by Van Blaaderen *et al.*[20] to make them suitable also for FRAP measurements[21,22] and direct imaging with CSLM.[23,24] As measured with static light scattering the particles have a radius of 200 ± 3 nm with a fluorescent core of 179 nm. The core contains about 8.7×10^5 dye molecules, assuming that all the added dye was incorporated in the silica. Dynamic light scattering gave a slightly smaller radius of 190 ± 5 nm. With transmission electron microscopy the polydispersity was found to be 5.5% relative to the mean. By index matching the particles in a suitable solvent mixture (ethanol/2-bromoethanol, ethanol/toluene), their refractive index could be determined at 1.449 (at 546 nm, 22 °C).

In short the synthesis proceeded as follows. First, 1.31 mmol of the fluorescent dye fluorescein isothiocyanate (FITC, isomer I, Sigma) was dissolved in 3 mL of distilled ethanol and allowed to react for 24 h with a 2-fold excess (2.73 mmol) of distilled 3-(aminopropyl)triethoxysilane (APS, Janssen). To a mixture of 2650 mL of distilled ethanol and 234 mL of 25% ammonia in a flask thermostated at 20 °C were added 114 mL of distilled tetraethoxysilane (TES, Fluka) and 2 mL of the APS–FITC mixture. After 24 h the particles were grown with 45 mL of TES and 1 mL of the APS–FITC mixture. Completion of the reaction was ensured by stirring the sol for 3 days. These core particles of radius 179 nm were then grown further to a final radius of 200 nm by the addition of 67 mL of TES.

The dispersion was then divided in three batches after which the particles were transferred to dimethylformamide (DMF, Baker) by repeated centrifugation and redispersion in DMF containing respectively, no added salt and 2.01×10^{-4} M and 1.00×10^{-3} M LiCl. For the no salt system the Debye length κ^{-1} was estimated from the conductivity assuming that trace ions are Li^+ and Cl^-. For the systems with added salt, κ was calculated taking into account the dissociation coefficient of LiCl (0.988 for 2×10^{-4} M and 0.972 for 1×10^{-3} M).[25] In Table 1 we show the conductivity and κa values of the solvents (a is the particle radius).

To obtain concentrated stock dispersions the particles were allowed to settle under gravity into a dense colloidal crystal after which most of the supernatant was removed. The particle mass density was then determined several times by drying a weighted amount of dispersion of known density. The value of 1.98 g/cm^3 thus found could then be used to determine the volume fraction of all concentrated dispersions by accurately measuring their density in a volumetric flask.

2.2. Rheological Measurements. Rheological measurements were performed using a Bohlin VOR controlled shear/strain rheometer equipped with a double concentric cylinder geometry of gap widths 1.5 and 2.2 mm. The geometry was thermostated at 25.0 °C and sealed to prevent evaporation of the solvent. The apparatus was calibrated using Newtonian calibration oils (NMI, Delft, The Netherlands) of known viscosity.

Since most of the samples were concentrated to above the melting volume fraction, we expect time-dependent effects to be important. To establish a reproducible shear history for all the samples, we were always careful to proceed in the following way. The sample was introduced into the geometry and allowed to thermostate while shearing at a rate of about 10 s^{-1} for some minutes. At this relatively high shear rate, a stationary stress response was always quickly established. Then a shear rate sweep up to about 200 s^{-1} and down again to 10 s^{-1} was performed. At each new shear rate the first 30 s constituted a delay time while during the next 30 s the instrument averaged the shear stress. The stresses measured during the downward sweep always coincided with the ones in the upward sweep, so no time-dependent effects were observed at these shear rates. The shear was then stopped to let the presheared sample equilibrate for at least 1 h. After that, the lowest possible shear rate (1.85×10^{-3} s^{-1}) was applied until the stress response had become stationary. For some samples this could take up to 15 min during which time the measured stress generally increased but would at times also temporarily decrease. When a stationary stress was reached, we always observed that upon further increasing the shear rate the corresponding stationary shear stress was reached within 30 s. Subsequently, a shear rate sweep up to 10 s^{-1} and down again to 1.85×10^{-3} s^{-1} was performed allowing a delay time of 60 s and a measuring time of 30 s at each shear rate. We verified that the results did not change if longer delay times were used. After the shear sweep the sample was equilibrated for 30 min, after which measurements of the viscoelastic properties were made. To this end the Bohlin rheometer generates oscillating strains and monitors the oscillating stress response, which in general contains in-phase and out-of-phase components. In this way, the storage and loss moduli, G' and G'' respectively, were measured in the frequency range $1-10^{-2}$ Hz for various strain amplitudes γ_0 in the range $10^{-3}-10^{-1}$. For the lowest strains G' and G'' generally are independent of the strain amplitude and the experiment is called linear viscoelastic. Finally, for some samples the stress relaxation function $G(t)$ was measured: A near step strain in the linear region was applied rising to its maximum in 0.2 s, after which the stress was monitored over time.

2.3. Observations Obtained by Using the Polarizing Microscope. Crystallized dispersions under shear were studied using a Zeiss axioplan polarizing microscope in transmission. The sample was observed between crossed polarizers so that multiple Bragg scattering identifies crystals as colored patches depending on their structure, orientation, and thickness.[18] Disordered systems scatter homogeneously and show almost no intensity. We mostly used a magnification of 25 times for making the (orthoscopic) images.

The samples were contained in thin flat glass cuvettes (Vitro Dynamics) of path length 0.2 mm, width 4 mm, and length 100 mm. The line of view (the optical axis of the microscope) was perpendicular to the 4×100 mm^2 face of the cuvette. Both ends of the cuvette were connected to tubes. One of the tubes was open to the air while the other was connected to the top of a gas burette half filled with water. The lower end of the buret was in turn connected to a wide funnel also containing water. If the levels in the buret and the funnel are equal, there is no pressure difference and the dispersion remains at rest. Lifting or lowering the funnel then creates a pressure difference causing the dispersion to flow one way or the other. The pressure remains constant since the flow through the cuvette is very small compared to the funnel's volume. The flow could be suddenly stopped by opening a valve in the tube connecting the cuvette and the buret.

In the experiments a sample was homogenized and introduced into the cuvette such that it completely filled the cuvette and part of the tubes connected to it. After the crystallites had filled

(18) Monovoukas, Y.; Gast, A. P. *Langmuir* **1991**, *7*, 460.
(19) Stöber, W.; Fink, A.; Bohn, E. *J. Colloid Interface Sci.* **1968**, *26*, 62.
(20) van Blaaderen, A.; Vrij, A. *Langmuir* **1992**, *8*, 2921.
(21) van Blaaderen, A.; Peetermans, J.; Maret, G.; Dhont, J. K. G. *J. Chem. Phys.* **1992**, *96*, 4591.
(22) Imhof, A.; van Blaaderen, A.; Maret, G.; Mellema, J.; Dhont, J. K. G. *J. Chem. Phys.* **1994**, *100*, 2170.
(23) van Blaaderen, A.; Imhof, A.; Hage, W.; Vrij, A. *Langmuir* **1992**, *8*, 1514.
(24) Verhaegh, N. A. M.; van Blaaderen, A. *Langmuir* **1994**, *10*, 1427.
(25) Prue, J.; Sherrington, P. J. *Trans. Faraday Soc.* **1961**, *57*, 1795.

the entire volume, a series of photographs were made at increasing flow rates. At each new rate the sample was allowed to flow for about a minute after which a more or less stable arrangement of crystals could be observed. In order to obtain unmoved photos, the flow had to be stopped for a short time, since with the samples used film exposure times of typically several seconds were needed.

3. Results

3.1. Rheology. In Figure 1 we show the flow curves (shear stress τ vs shear rate $\dot{\gamma}$) of the crystallized silica dispersions. Arrows indicate up/down shear sweeps. The samples are shear thinning from the lowest shear rate on, that is, they do not exhibit a low shear plateau in the viscosity. This is also the reason why we plot stress instead of viscosity since discontinuities are not easily detected in the overall shear thinning behavior of the dispersions. For all flow curves above a certain volume fraction, a hysteresis loop is observed roughly between 0.02 and 0.4 s^{-1} in shear rate. On increasing the shear rate the shear stress first increases slowly until at a certain point it remains constant or even decreases somewhat over about 1 order in the shear rate. After that, the stress starts to increase again with power law behavior at high shear rates. When the shear rate is subsequently decreased, the stress also decreases monotonously. Below 0.4 s^{-1} the stress is lower than during the upward sweep. This loop in the flow curve indicates a time-dependent effect caused by a structural rearrangement in the dispersion. Although the dispersion is shear thinning over the entire range of shear rates, the rearrangement is accompanied by an especially large drop in the viscosity since this quantity is defined as $\tau/\dot{\gamma}$. Following ref 17 we designate the shear stress at which the upward flow curve for the first time stops increasing as the critical stress τ_c. We will call the range 0.02–0.4 s^{-1}, where the stress is not an increasing function of shear rate, the critical shear rate range. As is seen in Figure 1, the beginning of this range does not vary systematically with either volume fraction or ionic strength. Its end, however, increases somewhat with volume fraction. We plotted the critical stress as a function of volume fraction in Figure 2, where it is seen to increase almost exponentially with volume fraction and more rapidly so at a lower ionic strength.

In Figure 3 we present some typical results of the viscoelastic measurements. It shows the storage and loss moduli (G' and G'' respectively) as functions of frequency for several strain amplitudes for a crystalline sample of volume fraction $\phi = 0.421$ at 0.001 M LiCl. For the lowest strains, G' and G'' were independent of the strain amplitude so the samples showed linear viscoelastic behavior. Figure 3 shows that for a colloidal crystal in a linear experiment G' is also independent of frequency in the range studied with the sample being almost completely elastic. The system is a viscoelastic solid. At larger strains the system increasingly behaves as a liquid: the storage modulus decreases while the loss modulus increases. Furthermore, the storage modulus becomes frequency dependent since the system finds ways to relax the stress through ever faster processes. This causes the storage modulus to decrease at the lower frequencies. The same is shown by the stress relaxation function of this sample (Figure 4): Only on time scales longer than 100 s the crystal finds ways to relax the stress and even after 3200 s the long-time (static) modulus G_0 was not yet reached. For short times the relaxation function has the same value as the storage modulus (for linear strains) at the frequencies

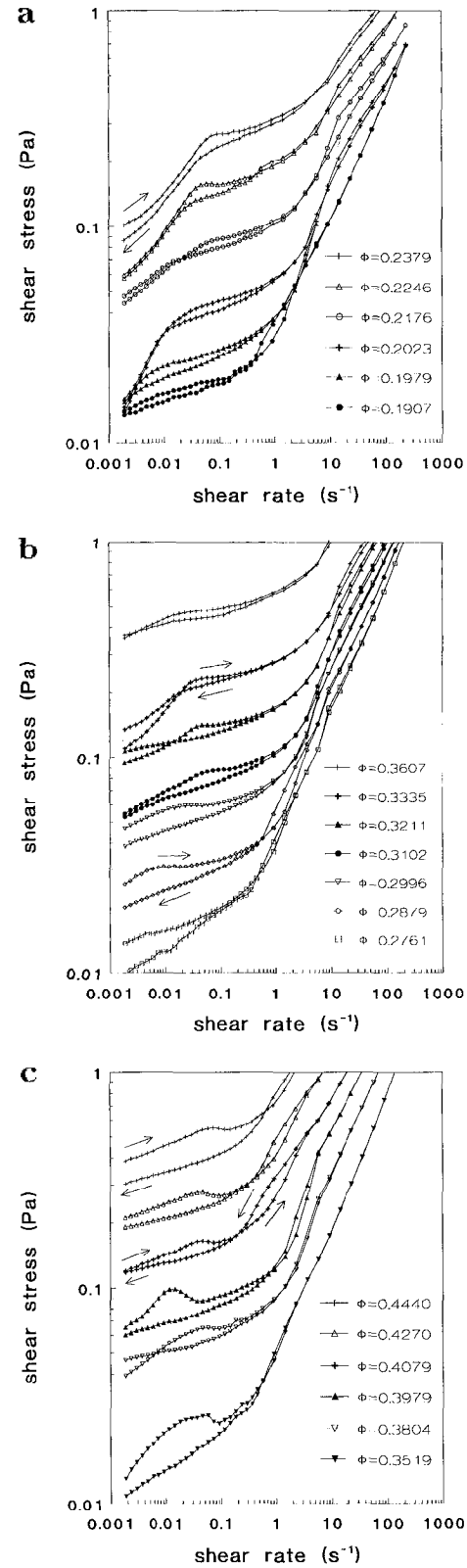

Figure 1. Several flow curves of the equilibrium crystalline samples: (a, top) no added salt; (b, middle) 0.0002 M LiCl; (c, bottom) 0.001 M LiCl. Arrows indicate the direction of the shear rate sweep.

in Figure 3. These results show that for the frequencies 0.01–1 Hz the linear viscoelastic experiments probe the colloidal crystal in the high-frequency limit. The corresponding storage modulus G_∞' was obtained from plots like the one in Figure 3 for all volume fractions and ionic strengths. The results are shown in Figure 2, which

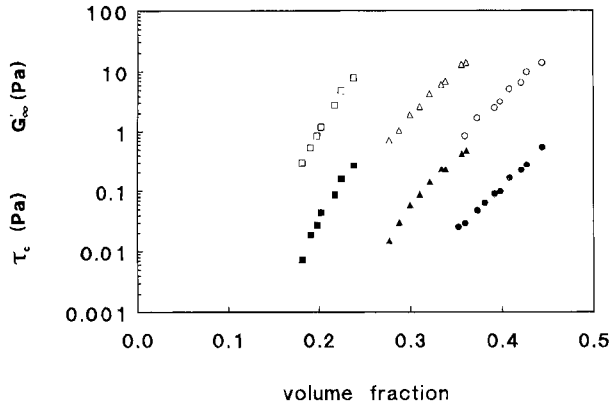

Figure 2. Critical stress (filled symbols) and high frequency limit of the storage modulus (open symbols) as a function volume fraction: squares, no added salt; triangles, 0.0002 M LiCl; circles, 0.001 M LiCl.

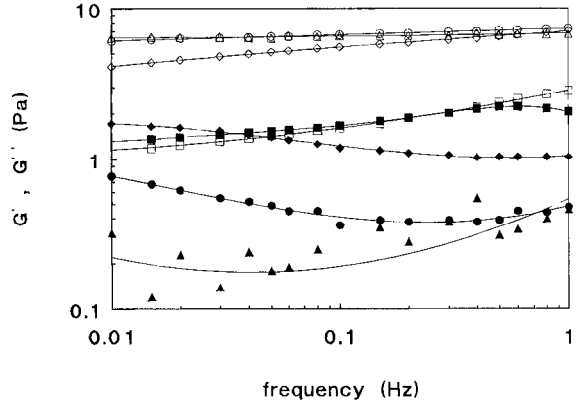

Figure 3. Storage modulus G' (open symbols) and loss modulus G'' (filled symbols) as a function of frequency for $\phi = 0.421$ (0.001 M LiCl) at several strain amplitudes γ_0: triangles, $\gamma_0 = 0.0027$; circles, $\gamma_0 = 0.013$; diamonds, $\gamma_0 = 0.026$; squares, $\gamma_0 = 0.083$. Lines were drawn to guide the eye.

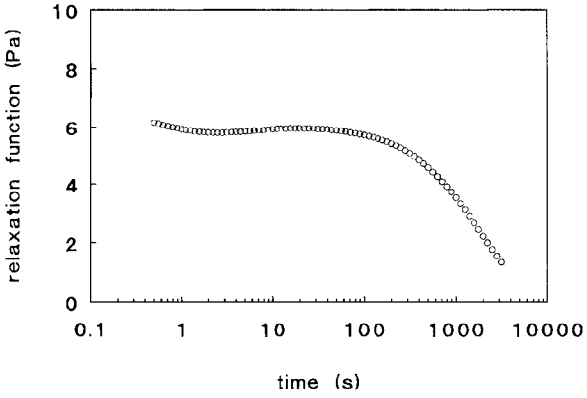

Figure 4. Stress relaxation function $G(t)$ of the same sample as in Figure 3. Strain = 0.0020, strain rise time 0.2 s.

suggests a close relation between τ_c and G_∞'. Indeed, Figure 5 shows that $\tau_c/G_\infty' = 0.033 \pm 0.003$, independent of volume fraction and ionic strength. This is similar to an observation by Chen and Zukoski[17] for concentrated latex dispersions. We will come back to this point in the discussion.

3.2. Polarizing Microscopy. Orthoscopic images made with the polarizing microscope are shown in Figure 6. The photos show the cuvette with a width of 4 mm from the left to the right on the photos. The flow is applied vertically, from the top to the bottom. As a result of the particles's fluorescence, the photos show a greenish hue. This is not caused by any diffraction phenomenon. The

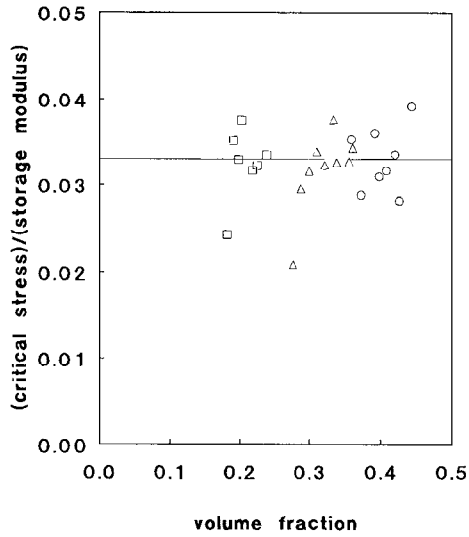

Figure 5. Critical stress divided by the high frequency limit of the storage modulus as a function of volume fraction: squares, no added salt; triangles, 0.0002 M LiCl; circles, 0.001 M LiCl. The horizontal line is the average value.

first photo (Figure 6a) shows a sample of volume fraction 0.28 (0.0002 M LiCl) after crystallites have completely filled the dispersion volume. The images in parts b–e of Figure 6 were made after applying an increasing pressure difference over this sample. We chose this series of photos because it was typical of the phenomena to be described shortly. Samples at a different volume fraction or ionic strength showed the same behavior. In Figure 6b the crystallites moved all at the same (though very small) speed through the cuvette, without visibly changing color, orientation, or size. This implies a very thin region of slip near the walls to establish the plug flow. Furthermore, two darker bands appear, to both the left and the right of the middle. At a higher pressure difference (Figure 6c) the uniform flow separates into a fast-moving middle region and two slower moving regions near both cuvette walls. Within these regions the flow velocity is uniform. The velocities of the left, middle, and right crystalline regions were measured with the help of an eyepiece equipped with a micrometer reticle and a stopwatch and are given in Table 2. The regions are separated by two bands where a velocity gradient is established which breaks up the crystals to a much smaller size as if they were ground between millstones. These shear zones occur at approximately the same position as the two darker bands in Figure 6b. At still higher pressures (Figure 6d) the shear zones do not visibly contain crystals any longer and grow at the expense of the crystalline regions (Figure 6e) until finally all crystals have disappeared and a Poiseuille-type flow is established. It should be noted here that the configuration of crystalline and sheared regions shown on any one of the photographs was quite constant in time. It only changed by varying the pressure difference over the sample.

For one sample ($\phi = 0.39$, 0.001 M LiCl) we interrupted the series of increasing flow rates at a point roughly corresponding to the situation in Figure 6d in order to let the dispersion recrystallize. The result is shown in Figure 6f, where it seen that in the shear zones large crystals nucleate that are elongated along the flow direction. This indicates that in these regions some anisotropic structure is retained.

4. Discussion

The silica dispersions used in this work were concentrated to above the melting volume fraction. After

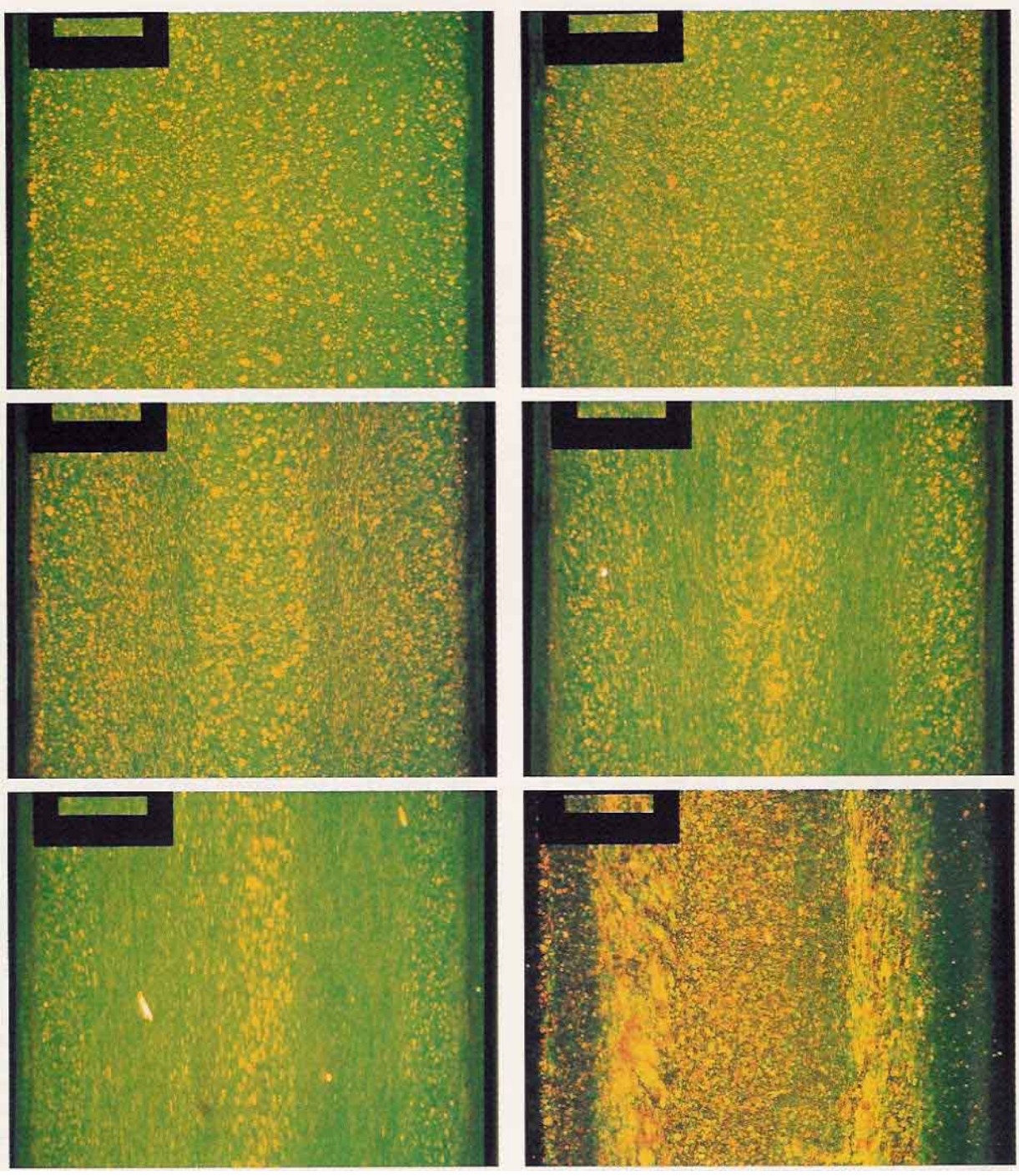

Figure 6. (a, top left) Photo of a sample of $\phi = 0.28$ at 0.0002 M LiCl made with the polarizing microscope. (b, top right; c, middle left; d, middle right; e, bottom left) Same after letting the dispersion flow through a cuvette at several rates. (f, bottom right) Sample of $\phi = 0.39$ at 0.001 M LiCl after flowing at an intermediate rate and then letting the dispersion recrystallize. (Occasional bright white spots are dust particles; a large one is seen in the left of Figure 6e.)

vigorously shaking a dispersion bright Bragg-reflecting crystallites were formed which filled the entire volume of the vessel. Although we did not attempt to determine the crystal structure, for the high volume fractions we used it is very probably fcc,[1,2] with perhaps some randomness in the stacking of the hexagonally close-packed layers as is seen for hard spheres.[26] Crystallization took place very rapidly: crystallites became visible within a period of seconds to minutes, depending on the volume fraction. Also depending on the volume fraction was their final size. Roughly, we can say that smaller crystallites were formed at higher volume fractions. The most concentrated samples appeared almost uniformly iridescent because of the very small crystallite size. In the range of volume

Table 2. Velocities of Crystalline Regions and Shear Rates Averaged over the Entire Width of the Cuvette and over Both Shear Zones for the Sample of Figure 6[a]

	velocity (μm/s)			average shear rate (s^{-1})		
figure	left	middle	right	overall	left	right
	24	45	17	0.023	0.060	0.067
6c	51	69	45	0.035	0.050	0.052
	85	150	76	0.076	0.11	0.18
6d	160	320	190	0.16	0.28	0.23
6e	380	570	380	0.29	0.24	0.22

[a] Some of the data correspond to the photos in Figure 6 as indicated.

(26) Pusey, P. N.; van Megen, W.; Bartlett, P.; Ackerson, B. J.; Rarity, J. G.; Underwood, S. M. *Phys. Rev. Lett.* **1989**, *63*, 2753.

fractions we used, we did not observe any evidence of a glass transition. Figure 6a shows a typical crystalline phase consisting of a mosaic of many crystallites of different size (10–50 μm), shape, and orientation. We were not able to make our dispersions nucleate in the cuvette in the form of one or a few large single crystals by shear alignment of particles prior to nucleation as is reported in ref 27 for a deionized latex. This procedure usually yielded a very heterogeneous system with groups of large and small and shear-oriented crystals at different places in the cuvette, probably because of the nonuniform shear rate. The shear-melting experiments with the microscope were therefore always done on homogeneously crystallized systems, such as the one shown in Figure 6a.

We shall proceed by discussing the microscopical observations first and then use these to interpret the rheological data.

In the experiments with the polarizing microscope we mainly observe two features. First, at the smallest flow rates, the crystallites remain intact while they all move at the same speed, but slightly darker bands are seen on both sides of the middle of the cuvette (Figure 6b). Second, at a higher flow rate, within the darker bands other bands are formed where crystallites break up, thus enabling the crystalline phase to flow. These shear zones dissipate most of the energy, thereby preventing damage to the remaining crystallites which remain in stable regions moving in a plug flow manner: one fast moving region in the middle and a slower one near each side. Upon further increasing the flow, the shear zones become wider at the expense of the crystalline regions. During this process the dark bands gradually disappear.

Before trying to explain these observations, we first consider the type of flow through the cuvette. For a Newtonian liquid a Poiseuille flow would set in. Since the cuvette has a rectangular cross section with sides 0.2 and 4 mm, the velocity gradient (*i.e.* shear rate) is steepest along its 0.2 mm axis. This direction coincides with the line of view of the microscope. We will refer to it as the lateral direction, being perpendicular to the field of view. The latter plane contains the transverse directions. One might expect the influence of the lateral shear rate on the crystallites to be the most severe. However, this turns out not to be the case. The photos in Figure 6 show that it is not this shear that causes melting, since melting is observed only in localized regions in the transverse direction. Furthermore, it would have caused the crystallites to become thinner. Since the color of individual crystallites depends directly on their thickness,[18] this process should have been accompanied by a change of color, which was not observed. This means that the crystallites move in a plug flow manner slowly slipping between the top and bottom walls of the cuvette and only the transverse shear causes melting. The origin of the slipping of crystallites could be a very thin layer of shear melted dispersion between the walls and the crystal. Since the dispersion is shear thinning at all shear rates measured, the viscosity in this layer would be strongly reduced, thereby facilitating the slipping motion. A possible explanation for the different flow behavior in the two directions may be related to the fact that in the lateral direction velocity gradients can be supported by only a few crystallites whereas in the wider direction many crystallites support the shear. While a single crystal tends to behave as a unit, an assembly of crystallites probably supports velocity gradients more easily due to the presence of many grain boundaries. This explanation assumes a qualitatively different flow behavior of a single crystal as compared to an assembly of crystals. The conclusion is then, that with the microscope we are studying the effect of shear flow on crystallites in the shear/velocity (∇,**v**) plane. This situation is rarely achieved in scattering experiments where one observes either the velocity/vorticity (**v**,**e**) or the shear/vorticity (∇,**e**) plane. In combination with the sensitivity with which individual crystallites can be observed, this makes the polarizing microscope well suited to study shear melting.

When crystals are subjected to a small shear force, they are first strained in order to resist the stress. When their elastic limit is reached, we expect the strained crystals to either form dislocations and then break or to reorientate to allow easier flow. This means that locally the resistance to stress drops and the crystals may be sheared further, giving rise to a kind of crack or shear zone. Since we see that the shear zones are preceded by slightly darker bands as viewed between crossed polarizers, it seems logical to seek the explanation of the darkening in a straining of crystal lattices. Since the wavelengths transmitted by the analyzer depend on the multiple Bragg scattering, we do expect straining to have an influence on color and intensity. Why this should turn out to be a darkening remains as yet unclear to us.

These observations show directly that in shear flow there can exist a stable coexistence between (poly)crystalline regions and sheared regions. The photographs provide no direct information as to the particle ordering in the shear zones. Scattering studies[6,7] indicate that shearing an fcc colloidal crystal causes particles to order into hexagonally packed sliding layers oriented perpendicular to the shear axis and with a close packed direction parallel to the flow. This is consistent with our observations since the sliding layers would be oriented parallel to the line of view and are not registered, so that they should not light up between crossed polarizers as do crystals. Although some small crystallites still seem to be present in the shear zones, it is clear that most of them have melted. A further clue to the structure in the shear zones is given by Figure 6f which shows that allowing the shear zones to recrystallize gives rise to elongated crystals aligned with the flow direction. This shows that at least some long-range order along the flow direction is retained in these regions, which is consistent with a sliding layers structure. A coexistence between an fcc structure and sliding layers has indeed been suggested recently by light scattering[8] and neutron scattering[10] studies. Since a single crystal in bulk would be expected to tumble and expose faces that are sensitive to shear melting, it must be stabilized by some mechanism if there is true coexistence between crystallites and sliding layers. One possibility for stabilizing crystals is provided by the walls of the container. Our observations suggest that another way for a crystallite to prevent melting is to be embedded in a large group of other crystallites. This explains why the coexistence is seen to consist of regions containing all the crystallites, separated by noncrystalline regions that support all of the shearing motion.

Interestingly, recent simulation results[28] show that under certain circumstances (above a certain shear rate and only when the so-called profile-unbiased thermostat was used) sheared colloidal crystals may localize all shear in a few planes. The regions between these planes consisted of a few layers of particles moving together as rigid blocks through the simulation box. Although on a much smaller scale, this process seems analogous to what

(27) Simon, R.; Palberg, T.; Leiderer, P. *J. Chem. Phys.* **1993**, *99*, 3030.

(28) Stevens, M. J.; Robbins, M. O. *Phys. Rev. E* **1993**, *48*, 3778.

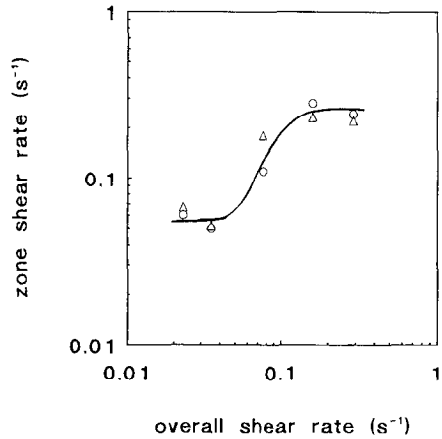

Figure 7. Average shear rate in the shear zones $\langle\dot{\gamma}\rangle_{shear}$ as a function of overall shear rate $\langle\dot{\gamma}\rangle$ with data from Table 2: circles, left shear zone; triangles, right shear zone. The line was drawn to guide the eye.

is observed in our experiments in that the crystal tries to localize shear to a small region.

In order to correlate the shear melting transition seen in the cuvette with the transition measured with rheology, we calculated the average shear rate $\langle\dot{\gamma}\rangle$ over the width of the cuvette for several situations, some of which are shown in Figure 6. The results, $\langle\dot{\gamma}\rangle$ = (velocity in the middle)/(half the width of the cuvette), are shown in Table 2. From the photos it is also possible to estimate the average shear rate in a shear zone $\langle\dot{\gamma}\rangle_{shear}$ from its width and the velocities of the crystalline regions bounding it. This number is also shown in Table 2. The values of $\langle\dot{\gamma}\rangle$ indicate that the shear melting starts at around 0.02 s^{-1} and is completed somewhat beyond 0.3 s^{-1}. These values coincide quite well with the critical shear rate range that is seen in the flow curves, showing that both are related to the same phenomenon. In Figure 7 we plotted $\langle\dot{\gamma}\rangle_{shear}$ as a function of $\langle\dot{\gamma}\rangle$. It shows that the shear rate in the shear zones suddenly increases from a lower to a higher plateau value as the overall shear rate traverses the critical shear rate range. This suggests that roughly two regimes can be distinguished during shear melting: one with a lower shear rate possibly related to the plastic deformation and breaking of crystallites and one with a higher shear rate related to the sliding layers structure.

These observations lead us to the following interpretation of the rheological data. When $\tau > \tau_c$ the crystallites can no longer resist the stress, start to break up in one or more places, and locally form a lower viscosity phase, probably consisting of sliding layers. This may cause a slight decrease in the shear stress. This lower viscosity phase is confined to sheets parallel to the flow/vorticity (**v**,**e**) plane and coexists with a polycrystalline phase. When the shear rate is increased, the extent of the shear zones increases at the expense of the crystalline regions. During this process the shear stress remains approximately constant implying that the polycrystalline regions melt at a constant (critical) stress. When the entire dispersion consists of the lower viscosity phase, the stress starts to increase with shear rate again. If one then lowers the shear rate, the system does not recrystallize during the course of the experiment but stays in the lower viscosity phase, giving rise to a hysteresis loop. Indeed, when the upward flow curve was measured immediately after a preshearing period, the system would retrace the lower stress branch of the flow curve instead of the upper one and would not show a critical stress.

In the geometry of our 0.2 × 4 mm^2 cuvette the regions where crystallites first started melting always appeared at about the same position. This fact is probably caused by an interplay of the preference of a fluid to establish a Poiseuille flow, the stabilizing action of the cell boundaries on the crystallites, and the size of the crystallites relative to the cell width. We mention here that for a sample containing 50–80 μm crystals in a 0.2 × 2 mm^2 cuvette the observations were qualitatively the same but with the shear zones starting out from the sides and growing inward as the flow was increased. Again, it is surprising that no melting was observed due to the large average shear rate in the lateral direction. In a rheometer with a concentric cylinders geometry the dispersion is subjected to a simple shear and there is no preferential position for shear melting to start. Therefore, the position of such a zone on the shear axis might be highly random, since it will depend on factors like the local packing of crystallites and their orientation, size, and lattice defects.

It may be questioned in how far the behavior of the microscope samples is comparable to that of the rheological samples, since only the latter were presheared for some time and then allowed to crystallize. We did this in order to apply a reproducible shear history to all samples and it probably causes the growth of orientated crystals (Figure 6f) or possibly even a large twinned single crystal.[29] We feel that factors like crystallite size, shape, orientation, and the presence of defects should indeed have consequences for the details of the flow in the sense that they determine the exact shear rate at which the melting transition occurs. They may be influenced for example by the long-time ripening of crystallites and could therefore be hard to control. This probably explains the relatively wide variety of shapes of the flow curves seen in Figure 1. Some show the structural transition in a much more pronounced way than others and there is no trend to be seen in the shear rate where the stress actually reaches its local maximum. What is more, we noticed that when the same sample was measured several times, the flow curve would also show some variation. However, despite variations in the exact form of the flow curve, the value of the critical stress was always reproducible to within 10%.

For shear rates below about 0.02 s^{-1} the dispersions are capable of sustaining a steady flow although they are entirely crystalline. A possible mechanism for this has been suggested by scattering experiments[7] and consists of layers of particles sliding past each other in a zigzag fashion without losing their three-dimensional ordering. With the microscope we did not observe any evidence for this process because, instead, at the lowest flow rates the crystals slowly moved en masse slipping along the cuvette walls.

At shear rates above about 0.4 s^{-1} the two-dimensional sliding layers structure is expected to melt further into a distorted liquid-like structure without long-range order.[4,7,8] This transition should be accompanied by a rapid increase in shear stress and this has indeed been reported once in the literature.[15] In our measurements something similar is seen in some of the flow curves in Figure 1, especially the ones corresponding to the highest volume fractions of the 0.001 M LiCl system. There, a second hysteresis loop occurs at shear rates above the critical shear rate range, only this time the upward flow curve passes below the downward one. This may be explained if on decreasing the shear rate the sliding layer structure does not immediately nucleate from the liquid, but when it does this is accompanied by a decrease in shear stress since the sliding layers offer less resistance to shear flow.

(29) Liu, J.; Weitz, D. A.; Ackerson, B. J. *Phys. Rev. E* **1993**, *48*, 1106.

It is not clear, however, why this loop is not seen in all the flow curves.

Simple mechanical models of crystalline solids predict a constant ratio between the shear stress at which the solid starts to deform plastically (elastic limit) and the shear modulus.[30] Depending on assumptions about the interaction between atoms the predicted ratio is between 0.16 and 0.033, whereas experiments show it to be several orders of magnitude smaller. The difference is caused by the motion of dislocations. In analogy, for aqueous latex dispersions Chen *et al.*[17] found a constant ratio of 0.035 ± 0.005 between the critical stress and the storage modulus. Our silica dispersions give $\tau_c/G_\infty' = 0.033 \pm 0.003$ (Figure 5), also independent of volume fraction and ionic strength. However, instead of G_∞' Chen *et al.* reported the use of the low frequency limit of the storage modulus G_0, determined from the recoverable strain at 1 s after the release of a small stress. This time scale is comparable to the one in our measurements (Figure 3). However, for our samples, and we suspect this to be the case for most colloidal crystals,[16] a measuring time of 1 s corresponds to the short-time (*i.e.* high frequency) limit as is also shown by Figure 4. Therefore, both works probably measured the same quantity.

Considering the fact that at τ_c the dispersion has severely shear thinned, one may wonder why τ_c should be strongly correlated with G_∞', a quantity which is a property of the equilibrium crystal. In light of the present finding that at τ_c only part of the crystal phase has melted, this becomes more clear: The storage modulus is the shear stress per unit of shear strain needed to displace layers of particles a small distance from their lattice positions, whereas the critical stress is the (steady) shear stress necessary for further taking these layers completely from the crystal into the sliding layers phase.

(30) Kittel, C. *Introduction to Solid State Physics*, 6th ed.; Wiley: New York, 1986.

5. Conclusions

It was shown that under the influence of a shear field a colloidal crystal phase breaks up into several regions moving in the flow direction at different rates. Along the shear direction these regions are separated by zones which together support all of the macroscopic shear. In these shear zones crystallites are destroyed and are probably transformed into a sliding layers structure. The coexistence between the regions seems to be quite stable in time. Recrystallization yields large aligned crystals in the shear zones, showing that some order is retained there. Increasing the shear rate causes growth of the shear zones at the expense of the crystalline regions. Rheologically the structural transition is characterized by a critical stress τ_c. During the transition the stress does not increase with shear rate until all crystallites have melted. The critical stress increases almost exponentially with volume fraction and more steeply so at a lower ionic strength. The critical stress divided by the high frequency limit of the storage modulus was found to be constant (0.033 ± 0.003) independent of volume fraction and ionic strength. The range of shear rates at which the transition takes place, however, did not show any clear dependence on these variables and also the exact shape of the flow curves showed some seemingly random variation. This may well have to do with factors like crystallite size, shape, and orientation and with lattice defects such as grain boundaries. The study of controlling the precise crystal morphology and its influence on mechanical and flow properties may have many interesting uses and requires more research.

Acknowledgment. This work is part of the research program of the foundation for Fundamental Research on Matter (FOM) with financial support of the Netherlands Organization for Scientific Research (NWO).